Acta Crystallographica Section D
Biological Crystallography
ISSN 1399-0047

A cautionary tale of structure-guided inhibitor development against an essential enzyme in the aspartate-biosynthetic pathway

Alexander G. Pavlovsky, Bharani Thangavelu, Pravin Bhansali and Ronald E. Viola*

Department of Chemistry and Biochemistry, The University of Toledo, Toledo, OH 43606, USA

Correspondence e-mail: ron.viola@utoledo.edu

Received 2 September 2014
Accepted 30 October 2014

PDB references:
*sp*ASADH–NADP + 4-nitro-2-phosphonobenzoate, 4r41; *vc*ASADH–NADP + 4-nitro-2-phosphonobenzoate, 4r5m; *sp*ASADH–NADP + 1,2,3-benzenetricarboxylate, 4r3n; *sp*ASADH–NADP + 3-(3-carboxypropyl)phthalate, 4r4j; *sp*ASADH–NADP + 3-(3-carboxypropenyl)phthalate, 4r5h; *sp*ASADH–NADP + 3-(2-carboxyethyl)phthalate, 4r54; *sp*ASADH–NADP + phthalate, 4r51; *sp*ASADH–2′,5′-ADP + 1,2,3-benzenetricarboxylate, 4r3w

The aspartate pathway is essential for the production of the amino acids required for protein synthesis and of the metabolites needed in bacterial development. This pathway also leads to the production of several classes of quorum-sensing molecules that can trigger virulence in certain microorganisms. The second enzyme in this pathway, aspartate β-semialdehyde dehydrogenase (ASADH), is absolutely required for bacterial survival and has been targeted for the design of selective inhibitors. Fragment-library screening has identified a new set of inhibitors that, while they do not resemble the substrates for this reaction, have been shown to bind at the active site of ASADH. Structure-guided development of these lead compounds has produced moderate inhibitors of the target enzyme, with some selectivity observed between the Gram-negative and Gram-positive orthologs of ASADH. However, many of these inhibitor analogs and derivatives have not yet achieved the expected enhanced affinity. Structural characterization of these enzyme–inhibitor complexes has provided detailed explanations for the barriers that interfere with optimal binding. Despite binding in the same active-site region, significant changes are observed in the orientation of these bound inhibitors that are caused by relatively modest structural alterations. Taken together, these studies present a cautionary tale for issues that can arise in the systematic approach to the modification of lead compounds that are being used to develop potent inhibitors.

1. Introduction

The aspartate pathway is the exclusive source for the synthesis of one-fifth of the amino acids that are required for protein biosynthesis in plants and microorganisms (Cohen, 1969; Viola, 2001). In addition to these indispensable amino acids, this pathway also produces several important metabolites that play crucial roles in essential developmental processes, including cell-wall biosynthesis (Van Heijenoort, 2001) and protective dormancy (Ragkousi *et al.*, 2003), and is also involved in virulence-factor production in certain microorganisms (Chen *et al.*, 2002; Lyon & Novick, 2004). The second enzyme in this pathway, aspartate β-semialdehyde dehydrogenase (ASADH), is located at the first branch point in this pathway, and the gene that codes for this enzyme has been shown by several studies to be part of the minimal set of genes that are absolutely required for bacterial survival (Gerdes *et al.*, 2003; Kobayashi *et al.*, 2003). This enzyme has become a target for the development of potential novel antibacterials, with selective inhibitors identified both through library screening (Gao *et al.*, 2010) and through substrate-

analog design (Cox *et al.*, 2001, 2005). The availability of an extensive set of ASADH structures from a number of different microbial species (Hadfield *et al.*, 1999; Faehnle *et al.*, 2005; Arachea *et al.*, 2010), as well as enzyme–substrate (Blanco *et al.*, 2004), enzyme–inactivator (Blanco, Moore, Kalabeeswaran *et al.*, 2003), enzyme–intermediate (Blanco, Moore & Viola, 2003; Faehnle *et al.*, 2006) and enzyme–product analog complexes (Pavlovsky *et al.*, 2012), have all been used to aid in the design of selective inhibitors.

More recent work has combined the power of fragment-library screening and molecular modeling to identify a structurally diverse group of small-molecule inhibitors that have shown selectivity in binding to bacterial and fungal orthologs of ASADH (Luniwal *et al.*, 2012). Despite this structural diversity, the binding of nearly all of these inhibitors has been guided primarily by electrostatic interactions between the negatively charged functional groups of the inhibitor and two highly conserved active-site arginine residues that play an important role in substrate binding (Blanco *et al.*, 2004). The current work reports the identification of a new set of inhibitors that bind in unique orientations within the active-site pocket. These structures show promise of development into high-affinity, selective inhibitors of this enzyme target once barriers to the optimization of inhibitor design have been overcome.

2. Materials and methods

2.1. Materials

Ethylene glycol (EG), polyethylene glycol (PEG 3350) and 24-well VDX plates were purchased from Hampton Research (Aliso Viejo, California, USA). MES buffer was purchased from Research Products International Corp. (Mount Prospect, Illinois, USA), dithiothreitol (DTT) was obtained from Gold Biotechnology (St Louis, Missouri, USA) and the substrates were purchased from Sigma–Aldrich (St Louis, Missouri, USA). The enzyme inhibitors in this study were either synthesized or were obtained from various commercial sources.

Aspartate β-semialdehyde dehydrogenase from the Gram-positive bacterium *Streptococcus pneumoniae* (*sp*ASADH) and the Gram-negative bacterium *Vibrio cholerae* (*vc*ASADH) were purified as described previously (Faehnle *et al.*, 2006; Blanco, Moore, Kalabeeswaran *et al.*, 2003; Moore *et al.*, 2002). The custom fragment library used in this study was assembled from a diverse set of 384 low-molecular-weight organic compounds containing substituted aromatic and heteroaromatic core structures (Gao *et al.*, 2010).

2.2. Enzyme crystallization and crystal complex formation

Crystal complexes of *sp*ASADH and *vc*ASADH with either nicotinamide dinucleotide phosphate (NADP) or 2′,5′-ADP were crystallized by the vapor-diffusion method, with the experiments being conducted in 24-well Linbro plates at room temperature. To 2 µl of a complex solution (enzyme at a concentration of ∼20 mg ml^{-1} and nucleotide at 4 m*M*) was added 1 µl well solution consisting of 14–20% polyethylene glycol (PEG) 3350, 0.1 *M* MES buffer pH 6.5, 0.1 *M* sodium acetate, 10 m*M* dithiothreitol (DTT), 3% ethylene glycol

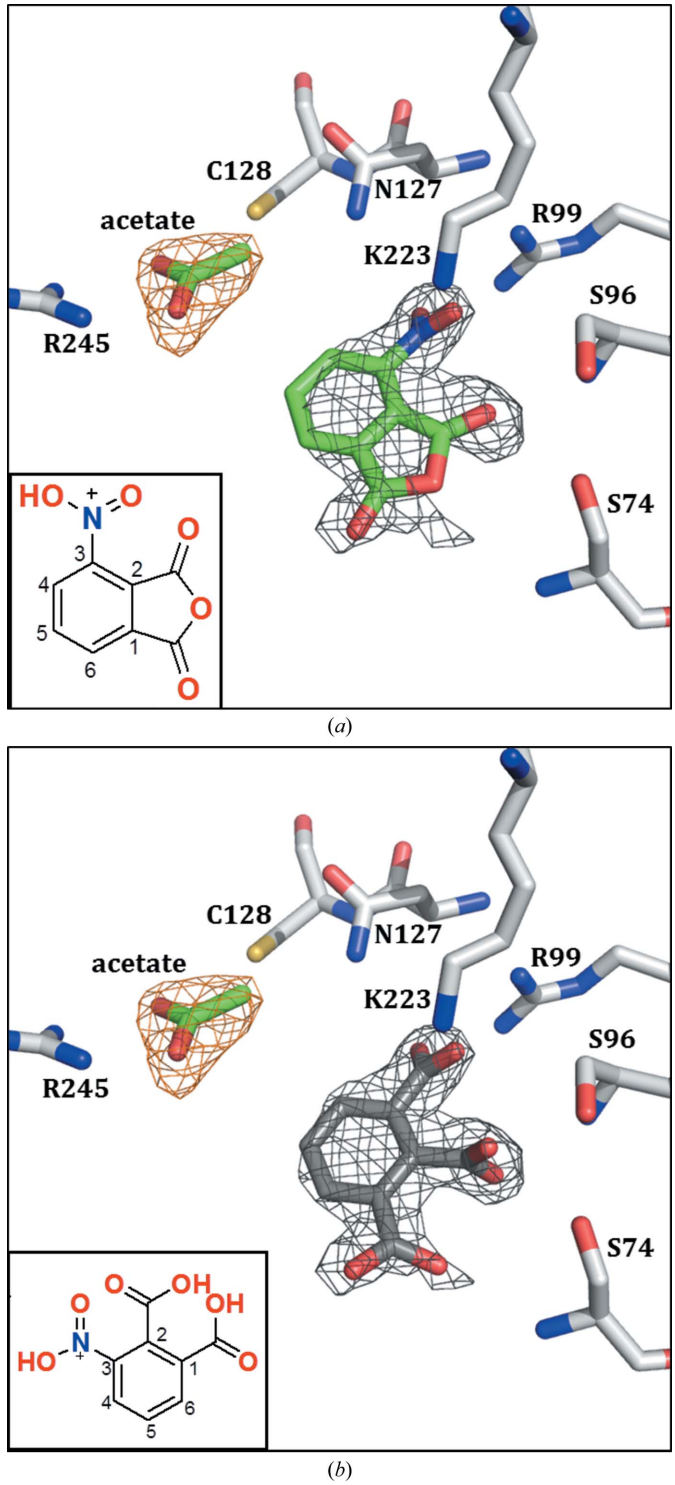

Figure 1
$mF_o - DF_c$ OMIT electron-density map (1.9 Å resolution, contoured at the 2.5σ level) of the *sp*ASADH binary complex with NADP superimposed with either (*a*) 3-nitrophthalic anhydride (green structure) or (*b*) 3-nitrophthalate (gray structure). The orange electron density in this structure corresponds to the acetate ion bound in the vicinity of Arg245.

Table 1
Data-collection and refinement statistics.

Values in parentheses are for the highest resolution shell.

Structure	Enzyme complex	K_i (mM)	Space group, unit-cell parameters (Å, °)	Resolution (Å)	R_{merge}	Completeness (%)	$\langle I/\sigma(I)\rangle$	R_{work}/R_{free}	R.m.s.d., bonds (Å)/ angles (°)	PDB code
I	*sp*ASADH + organic fragment library (cocktail No. 72)	—	$P2_1$, a = 59.8, b = 97.6, c = 64.2, β = 102.4	50–1.90 (1.97–1.90)	0.091 (0.221)	96.7 (89.6)	11.9 (4.7)	0.193/0.218	0.006/1.11	—
II	*sp*ASADH–NADP + 1,2,3-benzenetricarboxylate	1.0 ± 0.08	$P2_1$, a = 59.5, b = 97.7, c = 64.0, β = 102.5	50–1.35 (1.40–1.35)	0.061 (0.538)	95.3 (65.2)	19.7 (1.3)	0.131/0.161	0.010/1.65	4r3n
III	*sp*ASADH–2′,5′-ADP + 1,2,3-benzenetricarboxylate	1.0 ± 0.08	$P2_1$, a = 60.0, b = 98.4, c = 64.3, β = 102.4	50–1.90 (1.97–1.90)	0.074 (0.301)	87.0 (63.6)	12.7 (2.8)	0.189/0.233	0.009/1.32	4r3w
IV	*sp*ASADH–NADP + phthalate	3.8 ± 0.4	$P2_1$, a = 59.8, b = 98.4, c = 64.0, β = 102.6	50–1.80 (1.86–1.80)	0.151 (0.528)	98.8 (98.8)	7.8 (2.4)	0.176/0.198	0.006/1.28	4r51
V	*sp*ASADH–NADP + 3-(3-carboxypropyl)phthalate	2.4 ± 0.07	$P2_1$, a = 59.9, b = 98.8, c = 64.3, β = 100.9	50–1.50 (1.56–1.50)	0.073 (0.323)	92.5 (83.7)	26.1 (3.7)	0.151/0.190	0.006/1.34	4r4j
VI	*sp*ASADH–NADP + 3-(2-carboxyethyl)phthalate	2.2 ± 0.02	$P2_1$, a = 59.5, b = 98.8, c = 64.1, β = 101.2	50–1.81 (1.87–1.81)	0.120 (0.808)	99.0 (97.3)	26.0 (1.7)	0.184/0.220	0.008/1.38	4r54
VII	*sp*ASADH–NADP + 3-(3-carboxypropenyl)phthalate	4.2 ± 0.1	$P2_1$, a = 59.8, b = 98.4, c = 64.7, β = 100.3	50–1.80 (1.86–1.80)	0.105 (0.340)	95.2 (97.5)	7.5 (3.4)	0.184/0.231	0.010/1.54	4r5h
VIII	*sp*ASADH–NADP + 4-nitro-2-phosphonobenzoate	0.27 ± 0.02	$P2_1$, a = 59.6, b = 97.7, c = 63.9, β = 102.5	50–1.72 (1.80–1.72)	0.110 (0.530)	94.4 (83.5)	10.2 (1.8)	0.181/0.212	0.009/1.40	4r41
IX	*vc*ASADH–NADP + 4-nitro-2-phosphonobenzoate	0.076 ± 0.008	$P4_32_12$, a = b = 107.4, c = 152.8	50–1.88 (1.95–1.88)	0.123 (0.386)	97.7 (86.6)	10.6 (3.5)	0.170/0.197	0.007/1.25	4r5m

(EG), and the mixture was equilibrated as a hanging drop against 500 µl well solution. After about two weeks, the best formed crystals were soaked in a solution consisting of stabilization buffer [~15% PEG, 0.1 *M* MES, 0.1 *M* sodium acetate, 4 m*M* NADP (or 2′,5′-ADP), 3 m*M* EG] plus a single inhibitor at ~40 m*M* for 2–6 min followed by quick dip into cryoprotectant solution (the same as the soaking solution but with 25% EG) and were then cooled by plunging them into liquid nitrogen.

2.3. X-ray diffraction data collection

X-ray diffraction data for soaked crystal complexes were collected on the GM/CA-CAT beamline (Sectors 23B and 23D at the APS), with several data sets collected on our in-house R-AXIS image-plate detector mounted on an FR-E X-ray generator. All diffraction data were processed using *HKL*-2000 and scaled in *SCALEPACK* (Otwinowski & Minor, 1997).

2.4. Structure refinement

The structures of the ASADH–inhibitor complexes were determined by the difference Fourier technique (using PDB entry 3pwk for the *sp*ASADH complexes and PDB entry 3q0e for the *vc*ASADH complexes; Pavlovsky *et al.*, 2012). The enzyme coordinates were first refined as a rigid body against diffraction data limited to 3.5 Å resolution, followed by restrained refinement of data to the highest available resolution in *REFMAC*5 (Murshudov *et al.*, 2011). Finally, the solvent molecules and pertinent ligands were added and the structure was refined. Depending on the resolution level, the individual thermal parameters for the ligands were refined using either an isotropic or an anisotropic approximation.

3. Results

3.1. Inhibitor identification from fragment-library screening

Crystals of the ASADH complex with NADP were soaked with different cocktails of compounds from a custom organic fragment library. During X-ray screening of this library, one of the data sets obtained from these soaked crystals (cocktail No. 72) yielded additional electron density located at an unexpected position near the cofactor-binding site (Fig. 1*a*) despite the presence of bound NADP in this site (structure **I**; Table 1). The shape of the electron density at high resolution suggested the binding of 3-nitrophthalic anhydride, one of the four compounds in this cocktail, as the most likely inhibitor. However, the bridging O atom of the anhydride did not fit well within this electron density, and attempts to optimize the fit with the model structure led to a shift of the edge of the aromatic ring out of the electron density (Fig. 1*a*). The possible hydrolysis of this anhydride to the parent dicarboxylate (3-nitrophthalate) would lead to a compound with a significantly improved fit to the experimental density (Fig. 1*b*). Direct examination of this compound showed that 3-nitrophthalate is a moderate inhibitor ($K_i \simeq 2$ mM) of both *sp*ASADH and *vc*ASADH, while the freshly prepared anhydride does not inhibit either enzyme form. This observation suggests the potential binding of trianionic entities built on this core ring structure, which may yield improved ASADH inhibitors that could make unique binding interactions in the presence of the nucleotide cofactor. The additional electron density located close to the guanidinium group of Arg245 was fitted as an acetate ion resulting from the crystallization buffer. This binding pocket, which is normally occupied by the α-carboxylate of the amino-acid substrate, offers additional possibilities for inhibitor structural elaboration by fragment-based drug design.

3.2. Examination of inhibitor structural analogs

To test the importance of the binding interactions that are made by each anionic functional group, a series of structural analogs of 3-nitrophthalate were examined as potential inhibitors of this enzyme. Moving the position of the nitro group (4-nitrophthalate) or one of the carboxyl groups (5-nitroisophthalate), or eliminating the nitro group completely (phthalate), does not significantly alter inhibitor binding to ASADH from either bacterial species, with K_i values in the low-millimolar range for each of these structural analogs. However, more significant structural changes, such as replacing the carboxyl groups with nitro groups (1,3-dinitrobenzene), a combination of nitro and sulfonate groups (2,4-dinitrobenzenesulfonate), or the addition of halo substituents to phthalate (4-bromophthalate), are sufficient to eliminate binding to both enzyme orthologs.

Nitrophthalate analogs that showed at least 50% inhibition by kinetic assays when tested at 10 m*M* concentrations were soaked into crystals of the *sp*ASADH complex with NADP or 2′,5′-ADP and were then examined by X-ray diffraction (Table 1). Analyses of the electron densities in the active site of these crystal complexes showed that phthalate (K_i = 3.8 m*M*; structure **IV**) and 1,2,3-benzenetricarboxylate (BTC; K_i = 1.0 m*M*; structure **II**) each bind in the active site. In contrast, neither 4-hydroxyphthalate (K_i = 0.90 ± 0.02 m*M*) nor phthaldehyde (benzene-1,2-dicarboxaldehyde; K_i = 0.23 ± 0.04 m*M* *versus* *sp*ASADH and K_i = 0.017 ± 0.002 m*M* *versus* *vc*ASADH) were observed to be bound in these crystal-soaking experiments despite their good binding affinities.

As clearly indicated by the shape of the electron density, BTC binding is very well ordered in subunit *A* of *sp*ASADH (Fig. 2). This inhibitor forms an extensive hydrogen-bonding network with eight hydrogen bonds to protein atoms, including a bidentate interaction with the Arg99 guanidinium group, two bonds to the side-chain amine of Lys223 and bonding to the hydroxyl of Ser96 and its main-chain amide, as well as to the 2′-hydroxyl group of the nicotinamide ribose. The carboxylates in positions 1 and 2 of BTC are involved in the majority of these hydrogen-bonding interactions. The 3-carboxyl group has the weakest electron density, and appears to exist in two alternative conformations, each stabilized by forming hydrogen bonds to the 3′-hydroxyl of the nicotinamide ribose. In addition to these polar interactions, there are van der Waals interactions between the edge of the aromatic ring of BTC and the ribose adjacent to the nicotinamide that help to stabilize the orientation of the bound inhibitor.

3.3. Elaboration of inhibitor structures

Analysis of the electron density from each of this group of enzyme–inhibitor structures shows that in the complexes that were crystallized from acetate buffer an acetate ion typically binds in the active site through electrostatic interactions with Arg245. In the complex with BTC, the electron density in this site has the shape of a slightly distorted tetragon (Fig. 2), implying two orientations of acetate with equal occupancy.

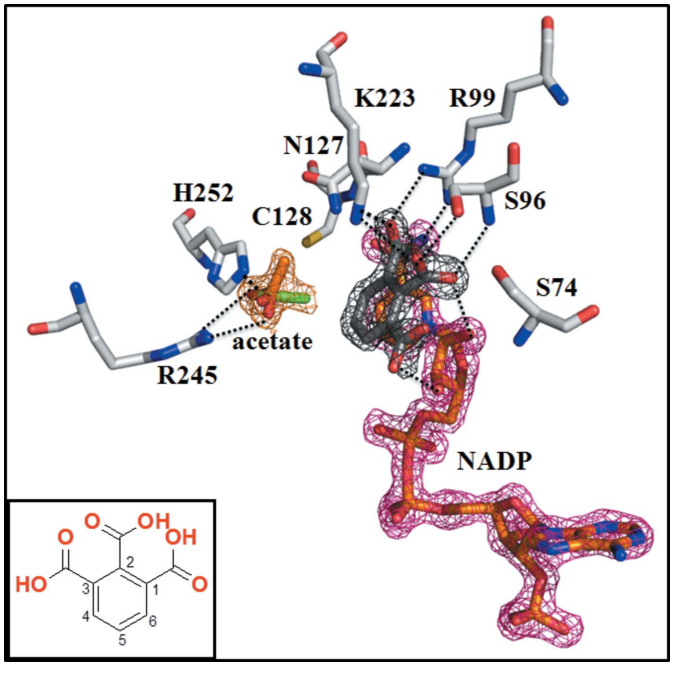

Figure 2
Binding of the 1,2,3-benzenetricarboxylate inhibitor (gray density) in the active site of the *sp*ASADH binary complex with NADP (magenta density) superimposed with the electron-density map ($2mF_o - DF_c$, 1.35 Å resolution, contoured at the 1.9σ level). Acetate is shown bound in two orientations with equal occupancy.

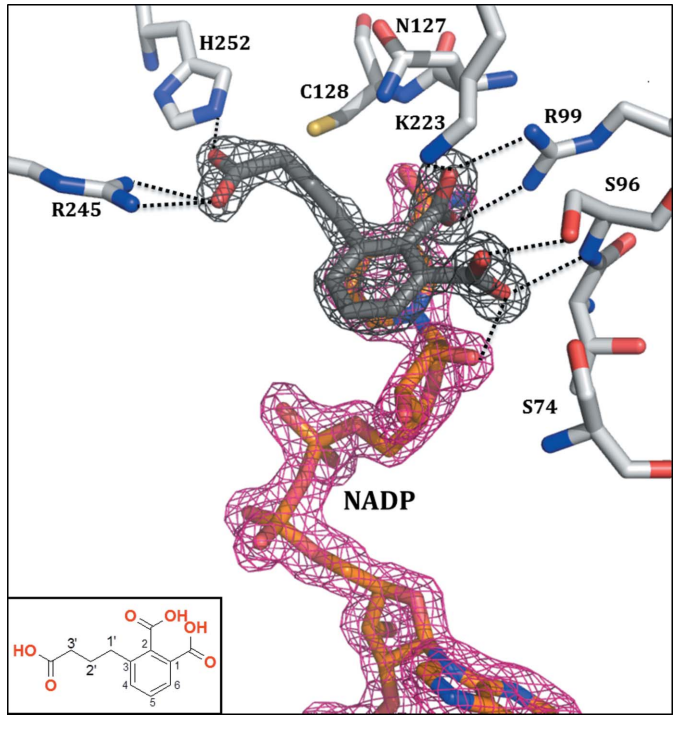

Figure 3
Binding of the 3-(3-carboxypropyl)phthalate inhibitor (gray density) in the active site of the *sp*ASADH binary complex with NADP (magenta density) ($2mF_o - DF_c$ map, 1.5 Å resolution, contoured at the 1.4σ level). The extended carboxylate side chain displaces the acetate that was bound in this site.

In both conformations the acetate O atoms form bidental hydrogen-bonding interactions with Arg245. In the few ASADH complexes where acetate is not bound, there is still density in this area consistent with two water molecules bound to the guanidinium group of this arginine. The identification of electron density in this region in all of the ASADH structures supports the importance of these binding groups (Ouyang & Viola, 1995), groups that could potentially be accessed to increase binding affinity by elaborating the structures of this benzoate family of inhibitors.

To achieve this goal, a linker was designed to extend the BTC structure into this acetate site located near Arg245. Initial modeling studies suggested that either 3-(2-carboxyethyl)phthalate or 3-(3-carboxypropyl)phthalate could access this site while still maintaining the BTC network of hydrogen-bonding interactions (Supplementary Fig. S1[1]). These compounds were synthesized and tested as potential ASADH inhibitors; however, each compound showed only modest inhibitory activity ($K_i \simeq 2$ mM). Structural analysis of these complexes shows that 3-(3-carboxypropyl)phthalate binds in a similar orientation (structure **V**) to that predicted from the modeling study (Supplementary Fig. S1). However, the overall electron density for this compound is weaker than that observed for BTC. Many of the hydrogen-bonding interactions that were observed with BTC are preserved in the binding of this new inhibitor, including a very similar hydrogen-bonding pattern between the aromatic carboxylate groups of 3-(3-carboxypropyl)phthalate and Arg99, Lys223, Ser96 and the 2′-hydroxyl of the nicotinamide ribose. The carboxypropyl side chain displaces acetate from its binding site by making new electrostatic interactions with Arg245 and His252 (Fig. 3). However, the strong hydrogen bond that was made to Asp127 in the binding of BTC is missing in this complex, as well as the interaction with the NADP ribose 3′-hydroxyl group.

Unexpectedly, the calculated electron density for the ternary complex with the 3-(2-carboxyethyl)phthalate analog shows a very different ligand-binding orientation (structure **VI**) compared with that observed for BTC and for 3-(3-carboxypropyl)phthalate. Instead of bridging into the acetate-binding site, the carboxyethyl group is oriented in the opposite direction. In this new orientation, this carboxyethyl group forms hydrogen-bonding interactions with the main-chain amides of Ser74 and, *via* a water molecule, Ser75 (Fig. 4). This reorientation still allows the aromatic carboxylate groups to form six hydrogen bonds to the same binding partners that are accessed by BTC and 3-(3-carboxypropyl)phthalate. However, acetate is not displaced by the binding of this inhibitor and remains bound in the same position as was previously observed.

3.4. Fine-tuning of the inhibitor structure

An unsaturated analog of the carboxyethylphthalate inhibitor, 3-(2-carboxyvinyl)phthalate, was synthesized in order to constrain the side-chain conformational flexibility, with the aim of increasing the likelihood of occupying the acetate-binding site. However, this analog did not show appreciable inhibition of ASADH, and soaking crystals of the NADP binary complex with this compound did not produce any electron density that could be assigned to a bound ligand. The corresponding unsaturated analog of the carboxylpropylphthalate, 3-(3-carboxypropenyl) phthalate, was also synthesized and soaked into crystals of the binary *sp*ASADH–NADP complex. Analysis of diffraction data obtained to 1.6 Å resolution shows that this inhibitor binds to the active site (structure **VII**) in a similar orientation to its saturated analog, although the propenyl group is more disordered (Fig. 5) compared with the electron density of the saturated side chain. This is a consequence of one of the bridging methylene groups making a very close and likely unfavorable contact with the backbone carbonyl of Gly159 (Fig. 5, red arrow), and is reflected in twofold weaker binding than the saturated analog (Table 1).

Because one of the terminal carboxylate groups of BTC is located in close proximity to the Arg99 guanidinium group, the site where the product phosphate is bound, substitution with a tetrahedral phosphonate or sulfonate group, while retaining the central carboxylate (in position 2) and eliminating the less involved carboxylate at position 3, could lead to improved binding affinity. A closely related compound, 4-nitro-2-phosphonobenzoate (Sigma–Aldrich), was found

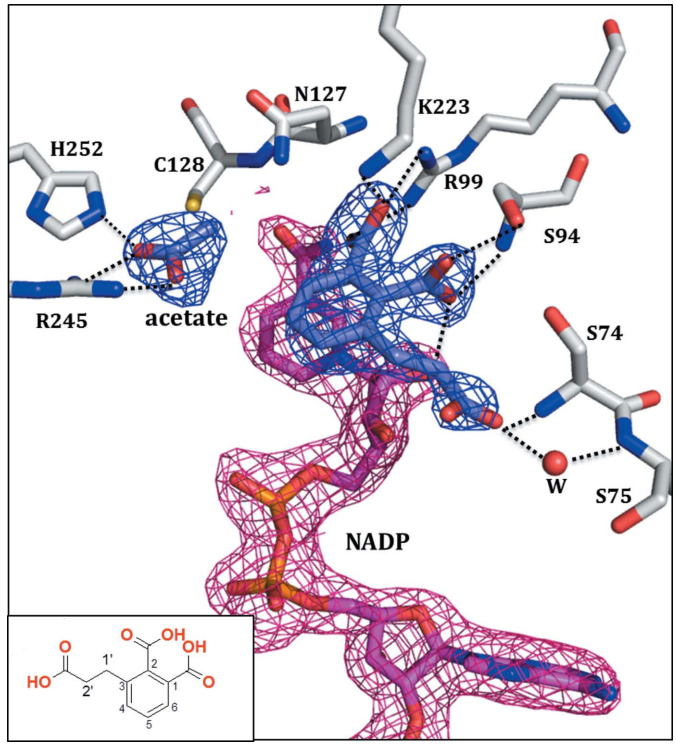

Figure 4
Binding of the 3-(2-carboxyethyl)phthalate inhibitor (blue density) in the active site of the *sp*ASADH binary complex with NADP (magenta density), showing the opposite orientation of the carboxyethyl group (1.8 Å resolution, contoured at the 1.2σ level).

[1] Supporting information has been deposited in the IUCr electronic archive (Reference: DW5116).

to be active against our ASADH target, with a fourfold improvement in binding affinity (K_i = 0.27 ± 0.02 m*M* *versus* *sp*ASADH) compared with *vc*ASADH. Analysis of the synchrotron diffraction data collected from an *sp*ASADH–NADP crystal complex soaked with this new inhibitor (structure **VIII**) reveals that this ligand does bind in the same active-site region (Fig. 6), but it is bound in a quite different orientation to that of BTC. The benzyl ring of the bound 4-nitro-2-phosphonobenzoate is nearly orthogonal to the orientation of the aromatic ring of BTC. Despite this reorientation, the polar atoms of 4-nitro-2-phosphonobenzoate are still in position to form up to nine hydrogen bonds, with the carboxylate group participating in four of these: one to the side-chain amide of Asn127, two to the terminal N atoms of Arg99 and another to the ε-amino group of Lys223. One of the O atoms of the phosphonate group interacts with the hydroxyl groups of Ser74 and Ser96 and with the peptide amide of Ser96, while another phosphonate O atom forms a hydrogen bond to the backbone amide of Ser74 (Fig. 6). Additionally, one of the O atoms of the nitro group binds to the backbone amide of Gly73. Unlike the binding of BTC, which forms van der Waals contacts with the ribose moiety of NADP (Fig. 7*a*), 4-nitro-2-phosphonobenzoate binding occurs closer to the active-site wall, in the region where the nicotinamide moiety is bound in the *sp*ASADH–NADP–BTC complex. As a result, the nicotinamide group is displaced and must occupy an alternative conformation through an ∼180° rotation around the O5′—αP bond. In this new, inactive conformation the α- and β-phosphate groups of NADP are still reasonably well ordered, while the ribose and nicotinamide moieties are now disordered with no interpretable electron density (Fig. 6). To compensate for the loss of interactions with the NADP cofactor, one face of the aromatic ring of the inhibitor makes new van der Waals interactions with residues 94–96 of the protein (Fig. 7*b*). Despite this reorientation, no bound acetate is found in the vicinity of Arg245. Instead, a single water molecule is found to occupy this position.

3.5. Differences in inhibitor binding between ASADH orthologs

Many of these phthalate derivatives show only moderate affinity for the *S. pneumoniae* form of ASADH, and have a comparable moderate affinity for the *V. cholerae* form. However, 4-nitro-2-phosphonobenzoate shows nearly fourfold stronger binding (structure **IX**) to *vc*ASADH (K_i = 0.076 m*M* *versus* 0.27 m*M* for *sp*ASADH), while several other derivatives show a tenfold or greater preference for *vc*ASADH. Replacing the nitro group of 3-nitrophthalate with an amino group (3-aminophthalate; K_i = 0.21 ± 0.04 m*M*) or extending the position of the carboxyl group (homophthalate; K_i = 0.46 ± 0.09 m*M*) leads to enhanced binding to *vc*ASADH, but with K_i values that remain in the 5 m*M* range *versus* *sp*ASADH. Conversely, replacing the nitro group with

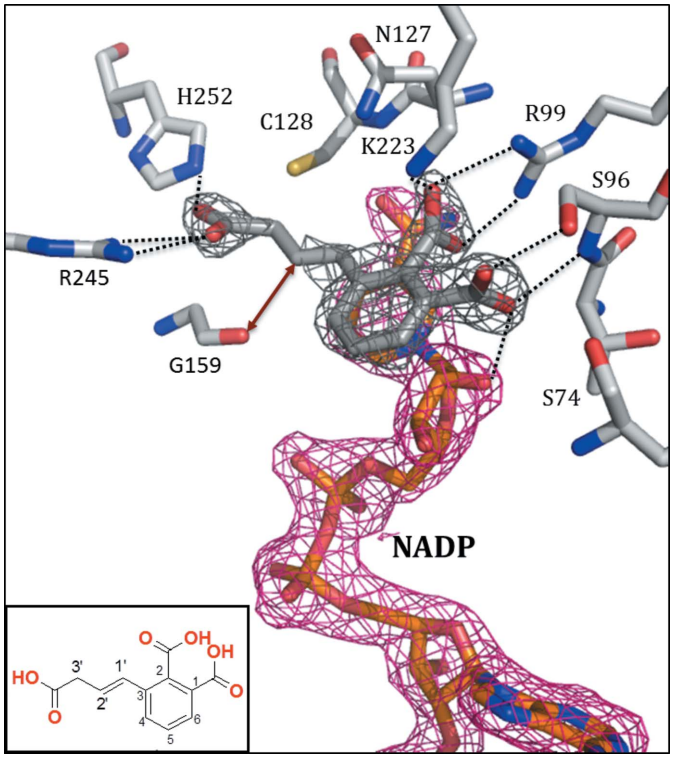

Figure 5
Binding of the 3-(3-carboxypropenyl)phthalate inhibitor (gray density) in the active site of the *sp*ASADH binary complex with NADP (magenta density, 1.8 Å resolution, contoured at the 1.2σ level). The red arrow indicates the tight contact with the carbonyl O atom of Gly159.

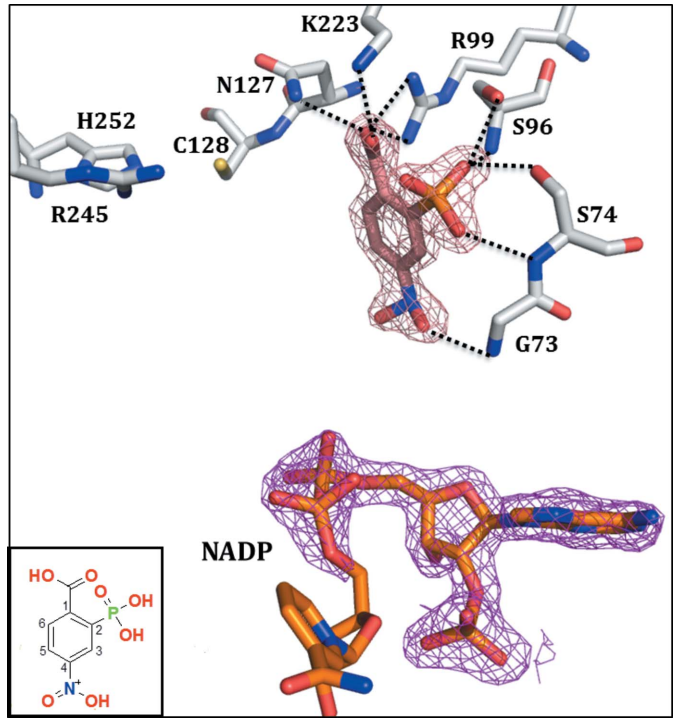

Figure 6
Binding of the 4-nitro-2-phosphonobenzoate inhibitor (pink density) in the active site of the *sp*ASADH binary complex with NADP (magenta density) superimposed with the electron-density map ($2mF_o - DF_c$, 1.6 Å resolution, contoured at the 1.7σ level). This structure shows the change in orientation of the inhibitor aromatic ring and the dramatically altered conformation of the bound NADP.

another carboxyl group (1,2,3-benzenetricarboxylate; BTC) actually leads to a slight improvement in affinity for *sp*ASADH, while essentially eliminating binding to the Gram-negative *vc*ASADH. In contrast, phthaldehyde is a 17 μ*M* inhibitor of *vc*ASADH, which is 14-fold greater than its affinity for *sp*ASADH.

At this stage, these lead compounds are not especially potent inhibitors of our target enzyme. This is not surprising since each of these inhibitors is a lower molecular-weight compound than the typical drug-like molecules, with fewer potential binding interactions. When adjusted for this size difference using the ligand efficiency metric (Hopkins *et al.*, 2004), these inhibitors have reasonably good LE values in the range 0.2–0.3 kcal per mole per heavy atom. An exception is the interaction of phthaldehyde with *vc*ASADH, with an excellent LE value of 0.65.

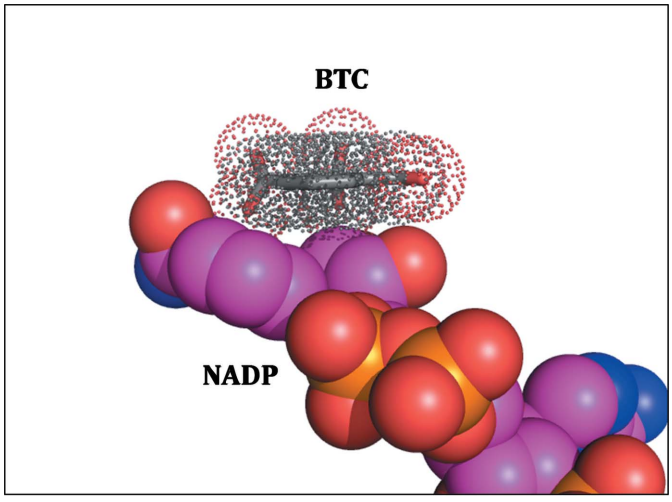

(*a*)

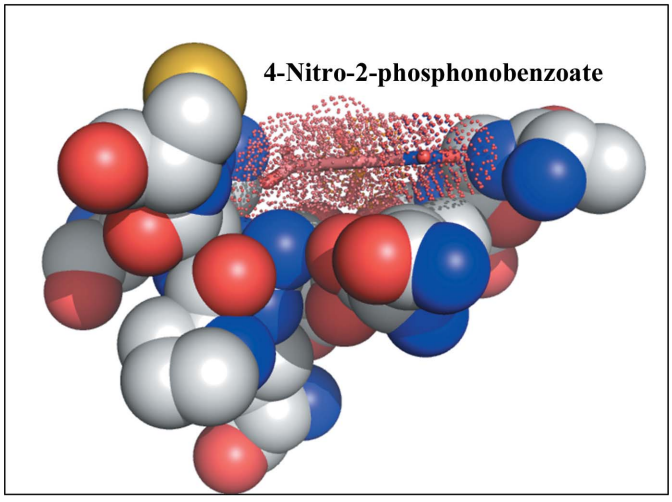

(*b*)

Figure 7
Space-filling model of the binding of inhibitors in the *sp*ASADH complex with NADP, showing the stabilizing van der Waals contacts. (*a*) Surface contacts between 1,2,3-benzenetricarboxylate (BTC) and the nicotinamide ribose of NADP. (*b*) Surface contacts between 4-nitro-2-phosphonobenzoate and the region of amino acids 94–96.

4. Discussion

4.1. Structure-guided optimization of inhibitor binding

The screening of fragment libraries is a cost-effective method to identify new chemical matter that can make productive binding interactions with a target protein. Structure-guided optimization of bound fragment inhibitors holds the promise of directing the elaboration of these initial core structures into adjacent binding pockets, leading to dramatic increases in affinity (Scott *et al.*, 2012). While this promise has been realised in a number of cases (Erlanson *et al.*, 2004; Howard *et al.*, 2006; Saxty *et al.*, 2007), frequently the expected affinity enhancements are not achieved and the reasons for the lack of success are not always obvious. In fact, a recent report on the non-additivity of substrate structural fragments (Barelier *et al.*, 2014) called into question the validity of the entire fragment-library approach. While this report specifically focused on the non-additivity of substrate-fragment binding, the conclusions in this paper also have implications for the use of the fragment-screening approach for inhibitor development.

The fortuitous hydrolysis of a component in a fragment-library cocktail led to the identification of a new core aromatic structure that binds to the active site of our target enzyme in an unusual orientation. The inhibition of ASADH by 3-nitrophthalate is driven by interactions with several charged and polar side-chain functional groups within the substrate-binding pocket. In addition, some important contacts with the NADP cofactor allow this inhibitor to bind with modest overall affinity but with good ligand efficiency. The presence of a bound acetate ion in an adjacent position in the active site provides guidance for the potential elaboration of this trianionic aromatic inhibitor to occupy this adjacent site. Incorporation of these additional binding interactions into a single structure should lead to a significantly more potent and selective inhibitor.

4.2. Barriers to inhibitor optimization

Structure analogs of this initial phthalate inhibitor were designed based on our detailed knowledge of the active-site binding interactions. Molecular modeling and docking studies have suggested several different side-chain designs and several potential orientations of these side chains that could occupy this acetate-binding site (Supplementary Fig. S1). The most promising of these derivatives were synthesized and tested as possible inhibitors of ASADH from *S. pneumoniae* and *V. cholerae*. Both 3-(3-carboxypropyl)phthalate and 3-(2-carboxyethyl)phthalate were found to be ASADH inhibitors, but unfortunately possess the same fairly modest, low-millimolar inhibition constants as that of the parent compound. While this failure to show improved affinity suggests that the introduced functional groups are not making any favorable binding interactions, in fact the structures of these bound inhibitors provides a very different picture. The longer carboxypropyl side chain does reach into the adjacent binding pocket and displace the acetate ion, as was predicted by modeling studies. However, the binding interactions with

Arg245 and His252 are somewhat distorted from the ideal distance and geometry (Fig. 3), with the donor and acceptor groups not optimally aligned as was observed with acetate binding in this site (Fig. 2). Also, the slight shift needed to accommodate binding at this site leads to a loss of one side-chain interaction (with Asn127) and one cofactor interaction (with the 3′-ribose hydroxyl group). Taken together, the compromises that are required to position this side chain are apparently sufficient to negate its potential contribution to improved affinity.

Decreasing this chain length by one carbon could possibly relieve some of these unfavorable binding interactions. Instead, this inhibitor homolog binds in a rotated orientation that positions the carboxyethyl group in the opposite direction, pointing away from the acetate-binding site. This new orientation is positioned through two hydrogen bonds, to a backbone amide group and to another amide through an intervening water molecule, that are apparently sufficient to stabilize this dramatically altered orientation (Fig. 4).

Because the central carboxylate of BTC occupies the phosphate-binding pocket of the aspartylphosphate substrate, the substitution of this planar carboxyl group with a tetrahedral oxyanion was speculated to have the potential to lead to an improved fit in this site. The commercially available compound 4-nitro-2-phosphonobenzoate was tested and found to be a good inhibitor of *sp*ASADH and an even better inhibitor of *vc*ASADH (Table 1). However, once again, this structural change led to a different orientation of the bound inhibitor. While most of the same hydrogen-bonding interactions that were observed with the structurally related inhibitors are still present in the binding of this inhibitor, it is now the benzoate carboxyl group that is bound in the phosphate-binding pocket and not the tetrahedral phosphonate group (Fig. 6). This compound is one of the better inhibitors among this aromatic structural family despite the absence of any of the stabilizing interactions that were present between BTC and the NADP cofactor. These van der Waals interactions between BTC and the cofactor (Fig. 7*a*) are replaced by improved surface complementarity between the aromatic ring of 4-nitro-2-phosphonobenzoate and the region of the protein containing amino acids 94–96 (Fig. 7*b*).

4.3. Effects on altered cofactor binding

The nicotinamide moiety in binary *sp*ASADH–NADP complexes is usually quite disordered, with either weak density or no density at all (Pavlovsky *et al.*, 2012). This conformational flexibility is reflected in the ternary complex with NADP and BTC. While these two ligands are in intimate contact when bound in subunit *A* of *sp*ASADH, in subunit *B* the nicotinamide moiety is primarily bound (with about 70% occupancy) in an alternative conformation that points outside the active site. This leads to a much shallower binding site for BTC and, although the set of hydrogen-bonding interactions with the enzyme are not dramatically changed from those observed in subunit *A*, without the steric support from the nicotinamide the inhibitor binding is less well ordered, as reflected by the missing electron density for the aromatic ring (Supplementary Fig. S2). Early work (Biellmann *et al.*, 1980) had suggested the possibility of cooperativity between subunits in ASADH. We subsequently identified a communication channel across the dimer interface to support this cooperativity (Blanco, Moore, Kalabeeswaran *et al.*, 2003) and showed diminished catalytic efficiency in an ASADH ortholog without subunit cooperativity (Faehnle *et al.*, 2005). The failure to induce the needed conformational changes upon inhibitor binding in one subunit will have an adverse effect on inhibitor binding in the adjacent subunit. This altered binding contributes to the lower than predicted affinity of this inhibitor towards ASADH.

A somewhat different phenomenon is observed when BTC is soaked into an *sp*ASADH complex with the NADP analog 2′,5′-ADP that lacks the nicotinamide and ribose moieties (structure **III**). In this case, the BTC inhibitor is bound in the active site of subunit *A* by forming a total of seven hydrogen bonds to the active-site functional groups (Supplementary Fig. S3). In the absence of the nicotinamide ring, a new bond is formed between the 3-carboxylate O atom of BTC and the backbone amide of Ser74. However, the resulting density corresponding to BTC is significantly less complete than the density observed in subunit *A* of the ASADH–NADP complex with BTC. Furthermore, no density is observed for this inhibitor in subunit *B* of the ASADH–2′,5′-ADP complex, again reinforcing the important role of the interactions with the cofactor in this mode of inhibitor binding.

5. Conclusions

Structural elaboration of initial fragment-library inhibitors has been found to be a viable approach for the development of potent and selective inhibitors against a target protein. However, barriers have frequently been encountered along the pathway to the production of a potent inhibitor. A large-scale derivatization program starting from a promising core structure can eventually produce sufficient advanced lead compounds to allow further inhibitor optimization. However, a better sense of how inhibitor binding is affected by subsequent derivatization can greatly assist in choosing the best pathway for inhibitor optimization.

In the case of our target enzyme, ASADH, initial fragment inhibitors were identified with only low-millimolar K_i values but with good ligand-binding efficiencies. Several routes, guided by modeling and docking studies, were explored for structural elaboration, including alterations in the nature and the position of the anionic functional groups and coupling with an adjacent bound fragment. While some improvements in binding affinity were achieved, some surprising and unexpected changes in the orientation of these bound inhibitors caused compromises in binding interactions that served to limit the optimal affinities that could be achieved. The binding of structurally related inhibitors in different orientations has previously been observed for the interaction of dipeptide inhibitors in different subsites in elastase (Mattos *et al.*, 1994), suggesting that this is potentially a more general phenomenon

then has been reported. In addition, the alterations in inhibitor binding in ASADH caused some unexpected changes in the binding of the NADP cofactor in the adjacent site that also limited the affinities that were attained. Understanding the driving forces that cause these altered binding modes will lead to improved design approaches to inhibitor optimization.

References

Arachea, B. T., Liu, X., Pavlovsky, A. G. & Viola, R. E. (2010). *Acta Cryst.* D**66**, 205–212.

Barelier, S., Cummings, J. A., Rauwerdink, A. M., Hitchcock, D. S., Farelli, J. D., Almo, S. C., Raushel, F. M., Allen, K. N. & Shoichet, B. K. (2014). *J. Am. Chem. Soc.* **136**, 7374–7382.

Biellmann, J. F., Eid, P., Hirth, C. & Jörnvall, H. (1980). *Eur. J. Biochem.* **104**, 59–64.

Blanco, J., Moore, R. A., Faehnle, C. R., Coe, D. M. & Viola, R. E. (2004). *Acta Cryst.* D**60**, 1388–1395.

Blanco, J., Moore, R. A., Kalabeeswaran, V. & Viola, R. E. (2003). *Protein Sci.* **12**, 27–33.

Blanco, J., Moore, R. A. & Viola, R. E. (2003). *Proc. Natl Acad. Sci. USA*, **100**, 12613–12617.

Chen, X., Schauder, S., Potier, N., Van Dorsselaer, A., Pelczer, I., Bassler, B. L. & Hughson, F. M. (2002). *Nature (London)*, **415**, 545–549.

Cohen, G. N. (1969). *Curr. Top. Cell. Regul.* **1**, 183–231.

Cox, R. J., Gibson, J. S. & Hadfield, A. T. (2005). *Chembiochem*, **6**, 2255–2260.

Cox, R. J., Hadfield, A. T. & Mayo-Martin, M. B. (2001). *Chem. Commun.*, pp. 1710–1711.

Erlanson, D. A., McDowell, R. S. & O'Brien, T. (2004). *J. Med. Chem.* **47**, 3463–3482.

Faehnle, C. R., Le Coq, J., Liu, X. & Viola, R. E. (2006). *J. Biol. Chem.* **281**, 31031–31040.

Faehnle, C. R., Ohren, J. F. & Viola, R. E. (2005). *J. Mol. Biol.* **353**, 1055–1068.

Gao, G., Liu, X., Pavlovsky, A. & Viola, R. E. (2010). *J. Biomol. Screen.* **15**, 1042–1050.

Gerdes, S. Y. *et al.* (2003). *J. Bacteriol.* **185**, 5673–5684.

Hadfield, A., Kryger, G., Ouyang, J., Petsko, G. A., Ringe, D. & Viola, R. (1999). *J. Mol. Biol.* **289**, 991–1002.

Hopkins, A. L., Groom, C. R. & Alex, A. (2004). *Drug Discov. Today*, **9**, 430–431.

Howard, N., Abell, C., Blakemore, W., Chessari, G., Congreve, M., Howard, S., Jhoti, H., Murray, C. W., Seavers, L. C. & van Montfort, R. L. (2006). *J. Med. Chem.* **49**, 1346–1355.

Kobayashi, K. *et al.* (2003). *Proc. Natl Acad. Sci. USA*, **100**, 4678–4683.

Luniwal, A., Wang, L., Pavlovsky, A., Erhardt, P. W. & Viola, R. E. (2012). *Bioorg. Med. Chem.* **20**, 2950–2956.

Lyon, G. J. & Novick, R. P. (2004). *Peptides*, **25**, 1389–1403.

Mattos, C., Rasmussen, B., Ding, X., Petsko, G. A. & Ringe, D. (1994). *Nature Struct. Biol.* **1**, 55–58.

Moore, R. A., Bocik, W. E. & Viola, R. E. (2002). *Protein Expr. Purif.* **25**, 189–194.

Murshudov, G. N., Skubák, P., Lebedev, A. A., Pannu, N. S., Steiner, R. A., Nicholls, R. A., Winn, M. D., Long, F. & Vagin, A. A. (2011). *Acta Cryst.* D**67**, 355–367.

Otwinowski, Z. & Minor, W. (1997). *Methods Enzymol.* **276**, 307–326.

Ouyang, J. & Viola, R. E. (1995). *Biochemistry*, **34**, 6394–6399.

Pavlovsky, A. G., Liu, X., Faehnle, C. R., Potente, N. & Viola, R. E. (2012). *Chem. Biol. Drug Des.* **79**, 128–136.

Ragkousi, K., Eichenberger, P., van Ooij, C. & Setlow, P. (2003). *J. Bacteriol.* **185**, 2315–2329.

Saxty, G., Woodhead, S. J., Berdini, V., Davies, T. G., Verdonk, M. L., Wyatt, P. G., Boyle, R. G., Barford, D., Downham, R., Garrett, M. D. & Carr, R. A. (2007). *J. Med. Chem.* **50**, 2293–2296.

Scott, D. E., Coyne, A. G., Hudson, S. A. & Abell, C. (2012). *Biochemistry*, **51**, 4990–5003.

Van Heijenoort, J. (2001). *Nat. Prod. Rep.* **18**, 503–519.

Viola, R. E. (2001). *Acc. Chem. Res.* **34**, 339–349.